ELSEVIER

Journal of Fluids and Structures 25 (2009) 420–430

JOURNAL OF FLUIDS AND STRUCTURES

www.elsevier.com/locate/jfs

Bottom slamming for a Very Large Floating Structure: Coupled global and slamming analyses

M. Greco[a,b,*], G. Colicchio[a,b], O.M. Faltinsen[b,c]

[a]*INSEAN, The Italian Ship Model Basin, via di Vallerano 139, 00128 Roma, Italy*
[b]*Centre for Ships and Ocean Structures (CeSOS), NTNU, Trondheim, Norway*
[c]*Department of Marine Technology & CeSOS, NTNU, Trondheim, Norway*

Received 19 September 2007; accepted 20 September 2008
Available online 30 November 2008

Abstract

An iterative Domain-Decomposition (DD) strategy is developed to examine the coupling between the global motions of a Very Large Floating Structure (VLFS) and bottom-slamming events. It combines (a) the linear-global analysis and (b) the fully-nonlinear description documented in Greco et al. [2008. Bottom slamming for a Very Large Floating Structure: Uncoupled global and slamming analyses. Journal of Fluids and Structures, this issue, doi:10.1016/j.jfluidstructs.2008.09.002]. Within the DD, (b) is used in an inner domain in the wave-side region of the VLFS, where bottom-slamming can occur. The initial and boundary conditions and the body motions are provided by the global analysis (a). The VLFS motions are then corrected using the global loads induced by slamming. The latter are obtained through a local analytical solution. Assessment of air-entrapment occurring during slamming is discussed, and a pressure criterion is proposed for slamming without air entrainment to switch from the analytical to the numerical evolution of pressure after the impact phase. Comparison with 2-D experiments shows a promising agreement.

Keywords: VLFS; 2-D potential flow; Coupled analysis; Domain-Decomposition strategy; Bottom-slamming with and without air cavity

1. Introduction

The present investigation aims to contribute to a deeper understanding of the slamming phenomenon on the bottom of Very Large Floating Structures (VLFS) due to their interactions with incident waves. The background and motivation of the study can be found in Section 1 of Greco et al. (2008).

A Domain-Decomposition (DD) strategy is developed to investigate the coupling between local phenomena and global platform behavior. It combines (a) the linear global VLFS model with (b) the fully nonlinear analysis described, respectively, in Sections 3 and 4 of Greco et al. (2008). Moreover the assumptions are the same as those given in Section 2 of that paper. The coupling is enforced through a converging series of iterations. A preliminary step in the DD development was reported in Greco et al. (2006) but the investigation of the occurrence of air-entrapment during

*Corresponding author at: INSEAN, The Italian Ship Model Basin, via di Vallerano 139, 00128 Roma, Italy. Tel.: +39 0650299343; fax: +39 065070619.
E-mail address: m.greco@insean.it (M. Greco).

0889-9746/$ - see front matter
doi:10.1016/j.jfluidstructs.2008.09.003

slamming, the pressure criterion proposed for slamming phenomena without air entrainment, and the iterative procedure for strong coupling are new contributions. The next section briefly recalls the main assumptions, describes the method and discusses the slamming studies performed. Then the main conclusions are drawn.

2. DD strategy

Here, the linear global solution and the nonlinear local analysis are coupled to investigate the effects of bottom slamming on the VLFS motions and *vice versa*. The structure is modeled as a barge. Head sea waves are investigated and the potential theory is applied to the flow which is assumed two dimensional in the plane of the platform longitudinal axis.

2.1. Solution algorithm

When considering the body motions, the platform length L represents an important parameter both for the local bottom-slamming problem and for modeling the whole platform. This means that generally the local phenomena depend on the global behavior of the platform and may in turn affect it. To limit the CPU-time requirements and still represent the bottom-slamming, a DD strategy has been developed to handle the global–local coupling.

From the global-motion point of view the effects of the local phenomena are modeled as additional time-varying loads $F_{\mathrm{loc},i}(t)$ on the right-hand-side of the global-motion equations [Eq. (1) in Greco et al. (2008)] which must be solved in the time domain. In general, they involve water-entry and water-exit phases of the platform, i.e. circumstances where the VLFS enters the liquid and goes out from the liquid, respectively. To evaluate $F_{\mathrm{loc},i}(t)$, an inner sub-domain is introduced around the upwave part of the platform (see Fig. 1). Within the sub-domain a fully-nonlinear analysis is performed with the Boundary Element Method (BEM) described in Section 4.1 of Greco et al. (2008), while in the rest of the fluid domain the nonlinear effects are neglected. The initial and boundary conditions, as well as the motions of the end of the platform lying within the sub-domain are given by the global solution. At any time instant the nonlinear solution furnishes the pressure along the wetted surface of the end part of the platform through the Bernoulli equation, then the local-pressure contribution is evaluated as difference between the nonlinear and linear pressure solutions. The local-pressure integration along the structure furnishes the generalized forces $F_{\mathrm{loc},i}$ (forces and moments) that can be inserted in the equations of motion to estimate the effect of local phenomena on the VLFS global behavior. The solution algorithm used within the DD strategy is shown in Fig. 2. Two alternative forms of coupling can be used: (a) a weak coupling, where the local problem receives the input data from the global linear solution and the resulting effects on the global motions are evaluated, and (b) a strong coupling. In the latter case an iterative process is performed between the local and global solutions until convergence of both global motions and local variables is reached. A suitable parameter for the convergence check of the local variables is represented by the impulse pressure estimated near the upwave end. Features of the linear and fully-nonlinear solvers relevant for the DD strategy are described in the following.

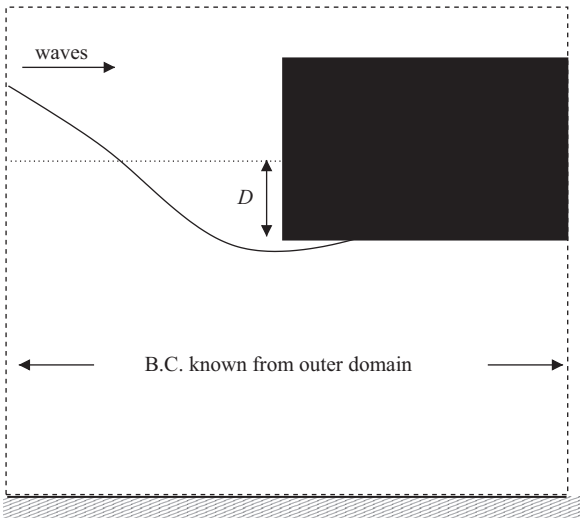

Fig. 1. Sketch of the local domain used for the bottom-slamming analysis within the DD method. D is the VLFS draft.

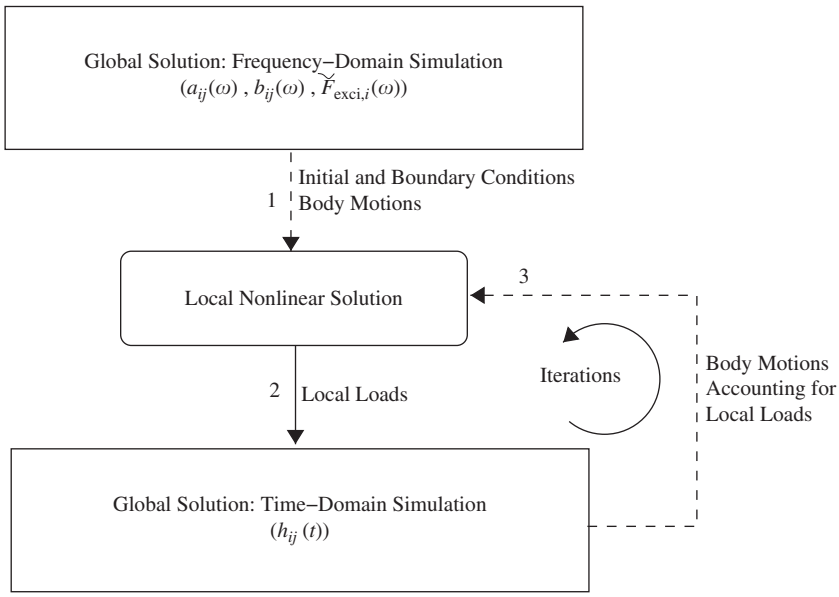

Fig. 2. Strategy for the iterative coupling between local and global solutions. $F_{\mathrm{exci},i}$ are the linear excitation loads.

2.2. Global motions in the time domain

To evaluate the global motions in the time domain all the terms in the modified equations of motion, i.e. accounting for $F_{\mathrm{loc},i}$, must be determined. In addition to the coefficients of the frequency-domain equations [see Eq. (2) of Greco et al. (2008)], the infinite-frequency added-mass terms $a_{ij}(\omega=\infty)$ must also be available. Here, $\omega=\infty$ is approximated with a value of ω high enough for its influence on the added-mass coefficients to be negligible. The correctness of this assumption has been checked against the results of a BEM solving the radiation problems in infinite/finite water depth with an infinite-frequency condition along the free surface.

The retardation response functions $h_{ij}(t)$ can be calculated in the two alternative ways:

$$h_{ij}(t)=-\frac{2}{\pi}\int_0^\infty \omega[a_{ij}(\omega)-a_{ij}(\omega=\infty)]\sin(\omega t)\,\mathrm{d}\omega \quad \text{or} \quad h_{ij}(t)=\frac{2}{\pi}\int_0^\infty b_{ij}(\omega)\cos(\omega t)\,\mathrm{d}\omega, \tag{1}$$

involving the convolution integrals of the added-mass and damping coefficients, $a_{ij}(\omega)$ and $b_{ij}(\omega)$, respectively. Both expressions have been discretized with a local linear interpolation of the load coefficients and performing a piece-by-piece analytical integration. The results are practically identical except near $\omega\simeq 0$ where the formula based on a_{ij} is less accurate. So the second of expressions (1) was adopted and checked by evaluating the added-mass and damping coefficients through the inverse transforms

$$a_{ij}(\omega)=a_{ij}(\omega=\infty)-\frac{1}{\omega}\int_0^\infty h_{ij}(t)\sin(\omega t)\,\mathrm{d}t \quad \text{and} \quad b_{ij}(t)=\int_0^\infty h_{ij}(t)\cos(\omega t)\,\mathrm{d}t. \tag{2}$$

The estimated h_{ij} were also verified against another numerical method in terms of the modal amplitudes predicted in steady-state conditions. For very small incoming-wave steepness, the DD method proved its ability to recover the linear solution in terms of the local free surface near the upwave portion of the platform and the local pressure on the VLFS bottom. In the case of nonlinear flow evolution involving water-exit and water-entry phases, the DD strategy gave reliable results in terms of free surface configurations [see Greco et al. (2006)] when compared with the fully-nonlinear solver described in Section 4 of Greco et al. (2008).

2.3. Bottom-slamming analysis

In the case of bottom slamming, the occurrence of air-entrainment phenomena can be overestimated when a single-phase model is adopted (Greco et al., 2008), and this represents a challenge for numerical solvers. In this framework the definition of an empirical criterion is useful. The analysis in Section 4.2 of Greco et al. (2008) suggests that the Euler number, *Eu*, could be a suitable parameter for such a criterion. Governing the air compressibility inside the cavity, *Eu* is

a measure of the air tendency to either escape and leave a wet structure (increasingly incompressible behavior as *Eu* increases) or be entrapped (more compressible behavior as *Eu* decreases). However, other physical parameters play a role due to the presence of the body (platform bottom). This is suggested by the experimental results in Yoshimoto et al. (1997), related to two geometrically identical models, with different rigidity, both able to deform but not to move rigidly. The Euler numbers, based on the velocity of the relative wave elevation, associated with slamming events of the more flexible model (A) were smaller than those connected with the stiffer one (B); however, model A did not experience any clear air-entrapment, while an air-cushion was observed in the case of model B. Yoshimoto et al. (1997) suggest the maximum bottom emergence $l_{d,\max}$ as a possible parameter for an empirical criterion, because they observed that $l_{d,\max}$ was larger for the stiffer model. However the values measured for $l_{d,\max}$ appear to be of the same order of magnitude for the two models, at least according to the example shown in Yoshimoto et al. (1997), so it would be difficult to define a criterion in terms of $l_{d,\max}$.

Because the time scales associated with the cavity closure are reasonably small, the distribution of the relative velocity of the cavity surface with respect to the platform bottom is more important than the bottom elastic deflections. A possible criterion could be obtained in terms of the position of the maximum relative velocity, say $V_{\max}$, along the cavity: the further downwave the location of $V_{\max}$, the less probable is air-entrapment. The numerical assessment of this criterion requires the use of a two-phase flow solution and has not been performed within the present analysis. It could however be of great practical importance and is left to a future research. For simplicity here it is assumed that for very small values of *Eu*, i.e. at full scale, a cavity entrapment occurs. When comparing with experiments, he cavity is modeled or neglected depending on what observed in the model tests.

Within the numerical solution, if the cavity is considered to be physical and kept in the simulation, the slamming pressure p_{slam} is directly handled by the BEM [see Section 4 of Greco et al. (2008)], so it is included in the pressure, say p_{inner}, predicted in the inner portion of the VLFS bottom by the nonlinear solver.

If the cavity is considered to be unphysical and then artificially omitted, the pressure induced by the impact cannot be handled by the BEM because the platform bottom is assumed to be fully wetted after the impact. However, the impact velocity V_0 and the impact angle β [see definitions in Greco et al. (2008)] predicted by the numerical solver at the impact instant can be used to estimate the impact pressure through the analytical impact solution p_{theo} outlined in Section 4.1 of Greco et al. (2008). Because p_{theo} is infinite at the spray root, $x = 2c$ (with x the distance along the bottom from the upwave edge), the maximum impact pressure predicted by the original Wagner (1932) theory is used as the limiting value for p_{theo}. This was done because (i) it does not require the composite solution between the global (from the BEM)

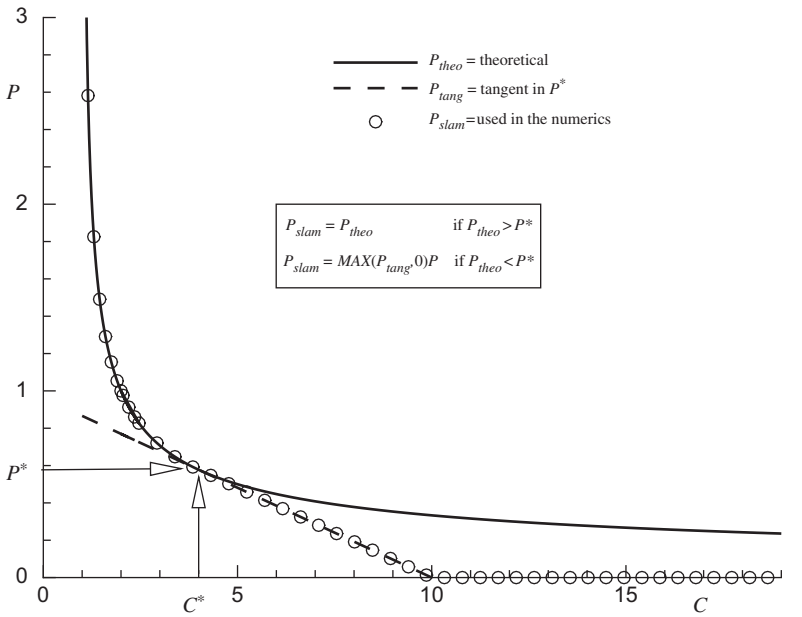

Fig. 3. Criterion used to estimate the slamming pressure p_{slam}. Nondimensional variables: $P = A_0 p/(\rho V_0^2)$, $C = 2c/x$, and related threshold variables: $P^* = A_0 p^*/(\rho V_0^2) \simeq 0.58$ and $C^* = 2c^*/x = 4$. p is the pressure, ρ the water density, $2c$ the spray root location and x the distance along the bottom from the wave-side edge. $A_0 = 3/2\tan(\beta)$ with V_0 and β, respectively, the impact velocity and angle. P_{tang} means the tangent to the curve P_{theo} in (C^*, P^*).

and the local [from the Wagner-type problem described in Faltinsen et al. (2004)] pressure solutions, and (ii) the maximum pressure is expected to be of the same order of magnitude as that predicted by the original Wagner theory.

In this case p_{inner} is estimated as follows: it is the sum of the hydrostatic contribution p_{hydr} and the slamming pressure p_{slam} at the platform-bottom locations $x<2c$, while elsewhere it is the value predicted by the nonlinear BEM. The solution p_{theo} does not account for the reduction of the entry velocity with time, so the slamming pressure p_{slam} coincides with p_{theo} only for the time interval in which it is larger than a specific value, say p^*. From then on p_{slam} is enforced to be linear and tangent to the p_{theo} curve. The value of p^* must be chosen in the range where the rate of change of p_{theo} reduces substantially, i.e. where the inertial terms due to slamming start to become limited. This criterion is illustrated in Fig. 3. After the spray root $2c(t)$ has covered a distance twice the value of the bottom-emergence length l_d at the impact instant, the predicted slamming global loads are smoothed out.

$F_{loc,i}(t)$ are obtained by subtracting the instantaneous linear pressure from $p_{inner}(t)$, and then integrating along the inner portion of the VLFS bottom (consistently with the definition of the generalized load components).

3. Applications

Here the DD strategy is applied to the case studied experimentally by Yoshimoto et al. (1997) for which a measurement of the bottom pressure time history is available (at the sensor P-1 located $x = 0.4L$ far from the upwave edge): the case refers to almost survival conditions with incoming waves $\lambda = 65D$ long and $H = 0.08\lambda$ high that interact with the more flexible model A. The experimental bottom slamming occurred without air-entrapment, and the same scenario has been enforced numerically. The coupling between bottom slamming and global motions of the platform is analyzed in terms of modal amplitudes and local pressures induced on the platform bottom.

Because local nonlinear phenomena may lead to small changes in the features of the slamming events (see later discussion), a single bottom event is selected and the induced loads are repeated in time as if they were periodic with the incoming-wave period and used as input for the global-motion analysis. An example is given in Fig. 4 for the force acting on the first beam mode. Both linear and slamming contributions are shown. The latter is introduced from a certain time instant (indicated by the vertical line in the plot) in the global motion equations and repeated periodically. The evolutions of the first-beam mode amplitude ξ_4 caused by the linear-exciting force, by its sum with the slamming load and by its sum with the load caused by both water-entry (including slamming) and water-exit phases are shown in Fig. 5. Within the considered time interval the slamming is responsible for a mean value of ξ_4 corresponding to few percent of the incoming-wave amplitude, while the water-exit phase has a negligible effect (see Fig. 6 showing the load contributions to the first beam mode associated with the inner-domain analysis). On a longer time scale the global motions show other features connected with the local phenomena. This is examined in Fig. 7 in terms of the time history

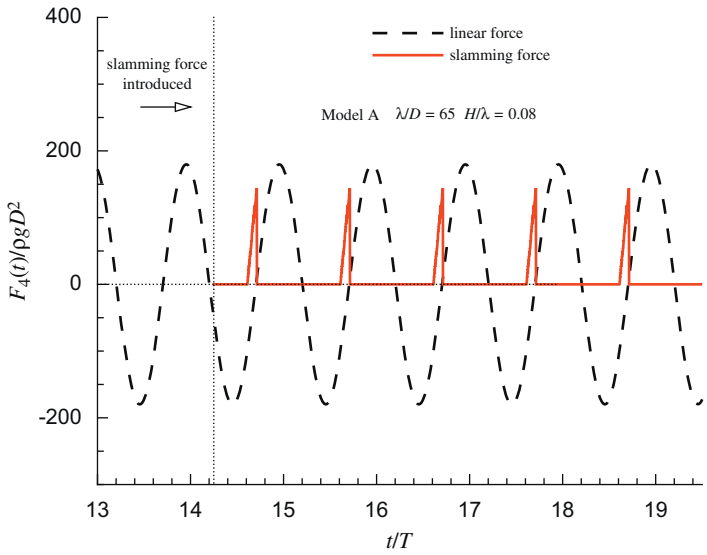

Fig. 4. Linear excitation and slamming forces for the first beam mode. ρ is the water density, g the acceleration gravity, and T the incoming-wave period.

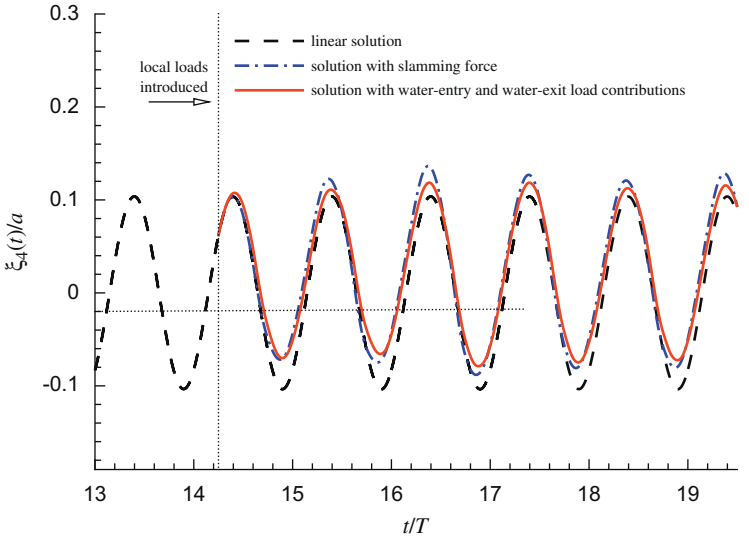

Fig. 5. Evolution of the first beam mode as obtained using the linear load (dashed line), the linear and slamming loads (dashed–dot line), and the linear load and local loads connected with both water-entry (and slamming) and water-exit phases of the platform bottom (solid line). $a = H/2$ and T are the incoming-wave amplitude and period.

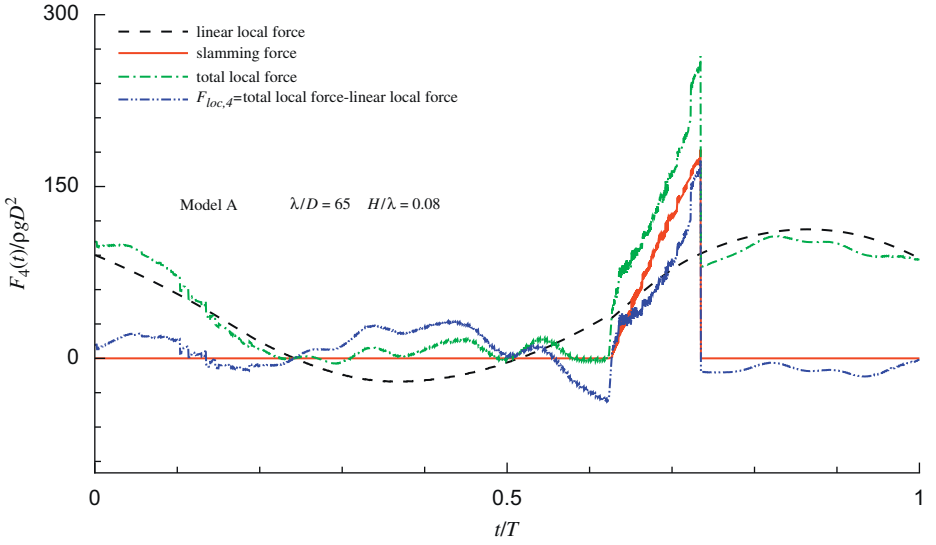

Fig. 6. Load contributions to the first beam mode associated with the inner-domain analysis: linear local term, slamming term, total local load (accounting for water-entry and water-exit phases) and $F_{\mathrm{loc},4}(t)$.

of the amplitudes of the first three beam modes; the corresponding shape functions, $\psi_j(x/L)$, are given in Fig. 8. All the modes experience a non-zero mean value due to the local phenomena and their evolutions are not characterized only by the incoming-wave frequency. The slamming occurrence excites also other components related to the natural frequencies of the modes and to the coupling among modes. The frequencies can be smaller, larger or comparable with the excitation frequency ω. In the present case for the first two modes they are much lower than ω and barely detectable from the plot due to the limited energy involved. For the third beam mode they are higher than ω and easily recognizable. The enrichment in frequency content may have effects on the safety and operations on a VLFS. The features of the elastic motions can be of concern for landing and take-off of airplanes on floating airports. The high-frequency vibration may induce a resonant vibration of sub-structures such as the control tower.

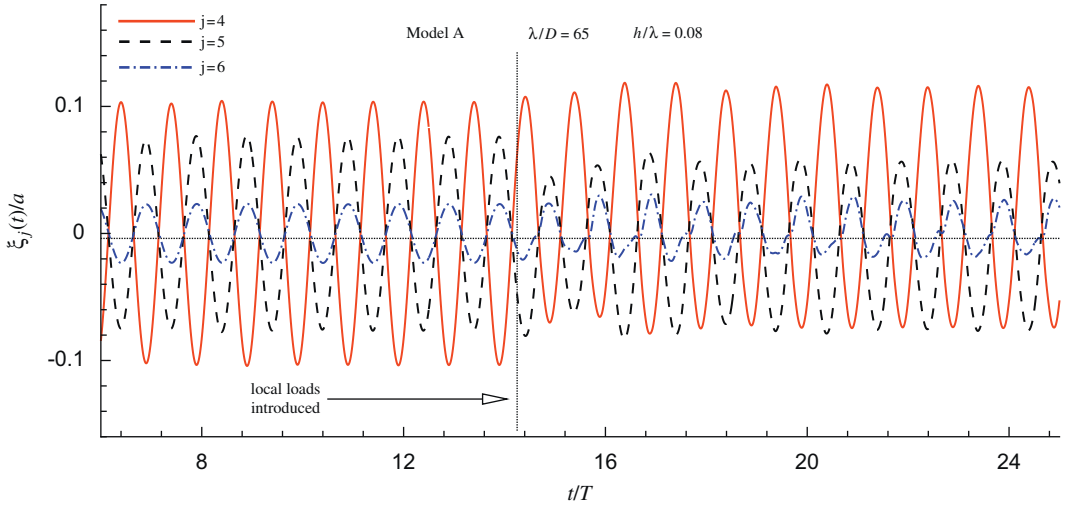

Fig. 7. Evolution of the amplitude of the first three beam modes as obtained using the linear and local loads.

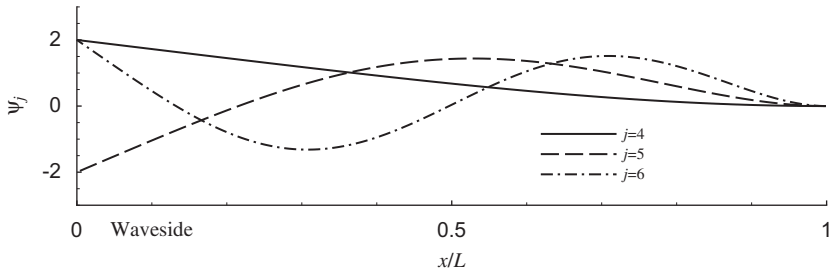

Fig. 8. Shape functions, $\psi_j(x/L)$, of the first three beam modes.

The results in Figs. 5 and 7 were obtained performing a strong-coupling DD strategy and correspond to the results of the third iteration between the global and local solutions. Figs. 9 and 10, respectively, examine the convergence of the coupling algorithm from a global and a local point of view. In particular, Fig. 9 shows the first beam mode as obtained after the first, second and third iterations and confirms a good convergence of the results after the second iteration. Fig. 10 gives the numerical pressure time evolution at sensor P-1. In the curve, $p = 0$ kPa means atmospheric pressure and $t = 0$ s represents the time when the simulations are started. The latter explains why the first impact differs more from the following ones. The solutions obtained after the first and second iteration show very similar higher-frequency oscillations which are not present in the linear solution. This suggests that the oscillations are caused by the slamming interactions with the global motions. The achievement of nearly convergent and steady-state global and local results suggests that cumulative errors in the mass and energy conservation are limited, even though no dedicated check has been done in this framework. The peak pressure associated with the slamming events shows variations both for different slamming events within the same curve and comparing different curves. The reason is that it is very sensitive to small variations of the impact angle β. On a physical level the results suggest a stochastic nature of the pressure peak. From the structural point of view the value of the pressure peak is of minor importance due to the short time involved, while the pressure impulse is of more concern. The duration of the impact load appears more repeatable within the sequence of slamming events for each curve and is consistent for the different pressure curves. These aspects are confirmed by the pressure-impulse results given in Fig. 11. They were estimated integrating the pressure in the time interval where the impact load matters (as indicated by the arrow in the enlarged view given in the plot). From the results, except for the first bottom-slamming event, the pressure impulse remains nearly the same for the different events and the values are close in the three simulations. The horizontal solid line in the plot represents a rough estimate of the pressure impulse associated with the pressure curve measured by Yoshimoto et al. (1997). This required the digitization of the experimental curve and suggests a promising consistency. The approximated experimental curve is shown in Fig. 12

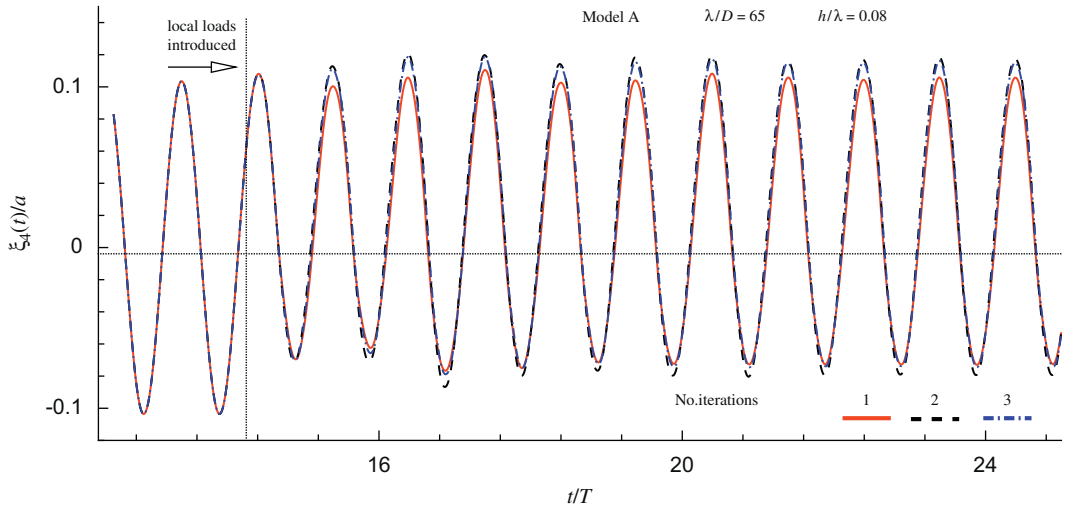

Fig. 9. Evolution of the first beam mode as predicted by the DD strategy at the first, second and third iteration between global and local solutions.

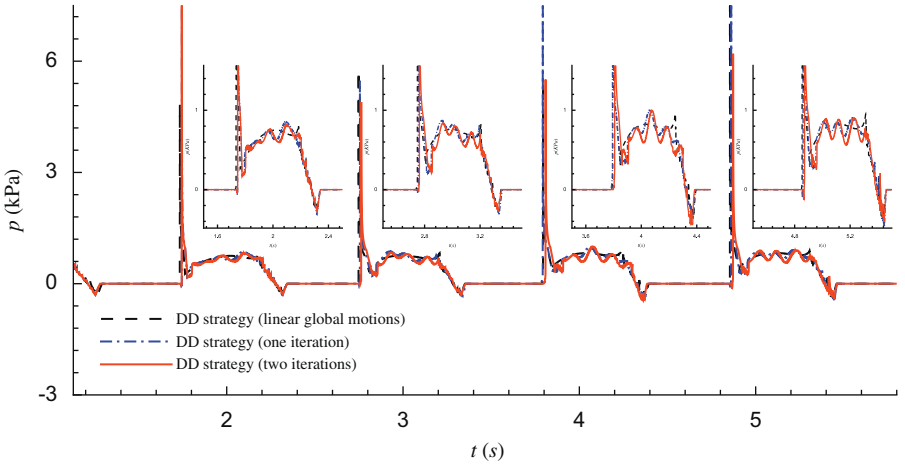

Fig. 10. Pressure evolution at the sensor P-1. Numerical results obtained using linear global motions (dashed line) and after one (dashed–dot line) and two (solid line) iterations of the DD strategy. The smaller plots in the figure give an enlarged view of the pressure behavior for the four periods examined.

(with the original curve given in Fig. 13) and compared with the numerical solution estimated after two iterations. The experimental curve is available only for one slamming event so it is not possible to investigate the repeatability of the pressure peak and general features.

Globally the agreement is satisfactory. Both measured and numerical pressures attain negative values before the pressure sensor becomes dry (i.e. zero pressure at the probe P-1). The latter occurs during the water turning at the upwave edge of the platform bottom, and is connected with the cross flow around this sharp corner. The numerics predicts a slightly different duration of this negative-pressure phase. A possible explanation is that vortex shedding probably occurred at the physical edge, but is not modeled in the analysis. The numerical model overestimates the maximum pressure caused by the impact, but it captures correctly the duration of the slamming load. This furnishes a validation of the criterion used to predict the duration of slamming loads for impacts without air-entrapment given in Fig. 3. After the impact both experimental and numerical results show high-frequency oscillations. However, in the experimental pressure, they appear more as jumps than as regular oscillations. The convergence analysis identified the

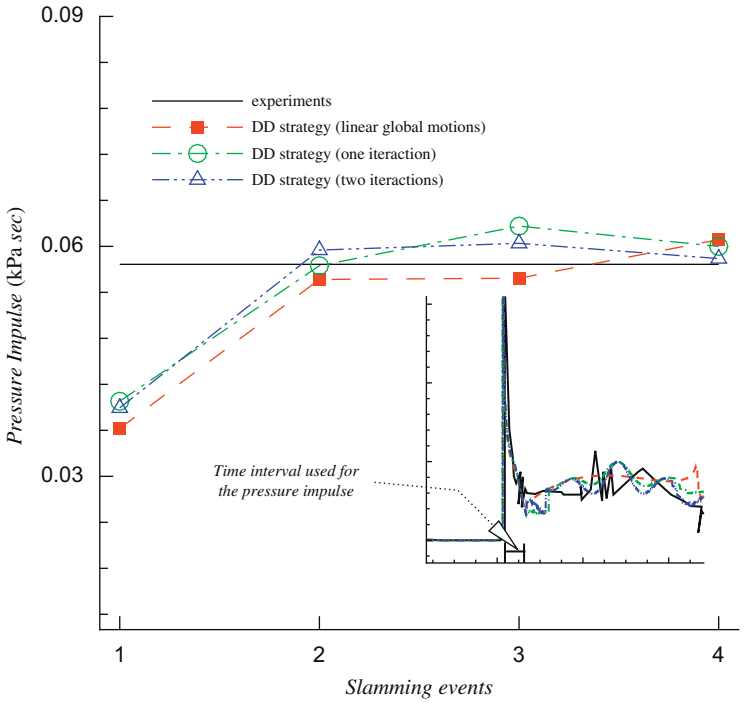

Fig. 11. Pressure impulse evaluated during the first four slamming events of the numerical solutions reported in Fig. 10. The horizontal solid line represents the rough estimate of the impulse pressure from the experimental pressure curve. The enlarged view in the plot shows the time interval used for the pressure time integration.

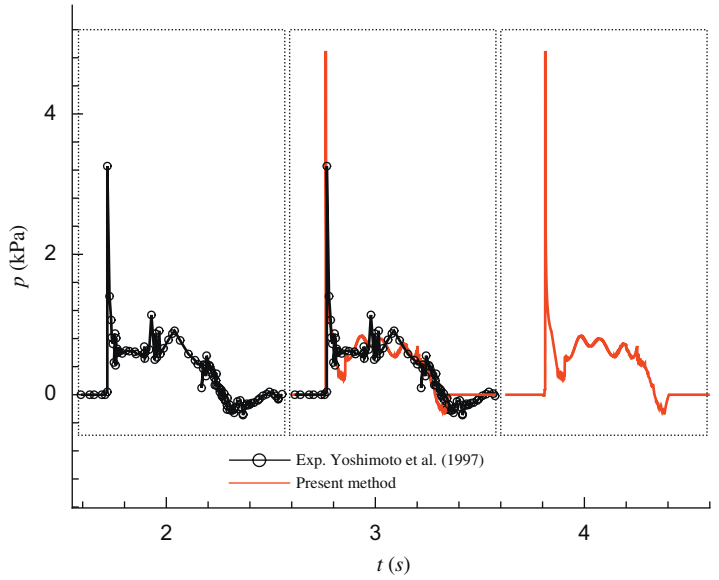

Fig. 12. Pressure evolution at the sensor P-1. Experimental and numerical results (second bottom slamming) after two iterations. For sake of clarity the experimental and numerical pressure curves are given separately at the left and right of the plot, respectively.

coupling between global motions and local slamming as the main reason for the oscillations in the numerical prediction. The differences between numerical and experimental oscillatory features can be partially associated with structural damping not modeled in the numerical analysis. Further, the local details of the structure matter and they are not taken

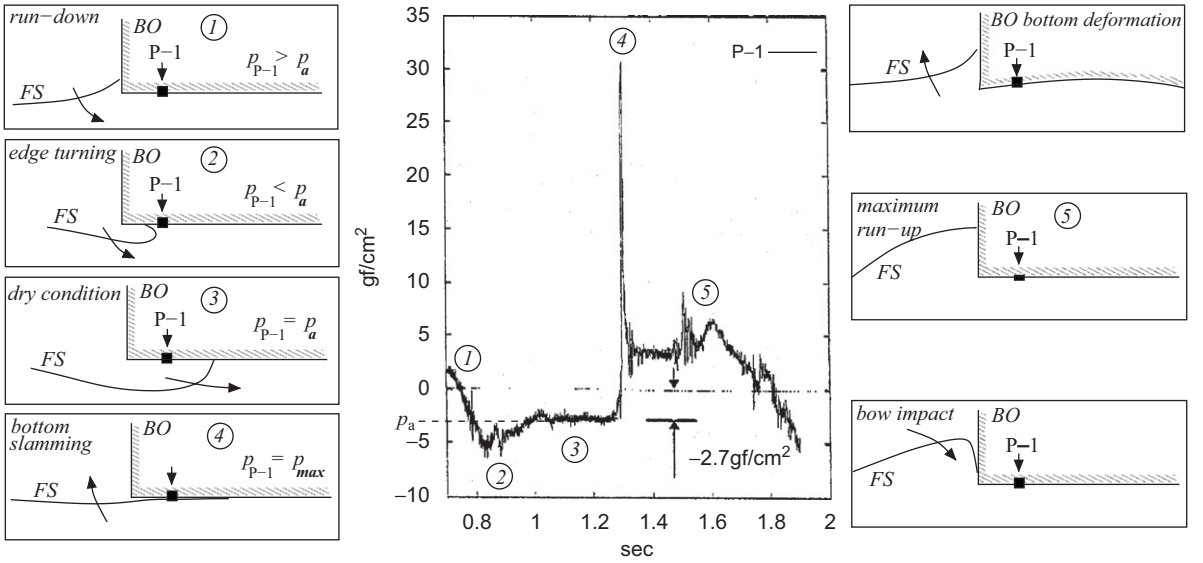

Fig. 13. Pressure measurements by Yoshimoto et al. (1997) at location P-1 and physical interpretation of the experimental behavior from the numerical analysis.

into account in the present analysis. Other phenomena responsible for sudden pressure variations are impacts occurring at the platform bow (i.e. at the upwave end). A tendency to bow impact was clearly observed in the numerical prediction during the water run-down phase, as documented by Greco et al. (2006). Because this was not the focus of the study, in the numerical model the bow impacts were prevented by cutting the locally steep free surface and connecting the remaining free surface to the body. The numerical cut induced a small jump in the bottom pressure which is hidden in the converged pressure curve due to the earlier oscillations induced by the interactions between the slamming and the elastic motions. However the jump is detectable in the numerical pressure curve obtained using the global linear motions (cf. Fig. 10). This jump is consistent with the later jump shown by the experimental pressure.

On the basis of the present studies the features of the pressure evolution during impact events can be identified. They are labeled by numbers in Fig. 13 on the pressure evolution measured by Yoshimoto et al. (1997): the run-down phase (1) is responsible for a pressure reduction leading to values even lower than the atmospheric pressure during the water turning around the upwave edge of the platform bottom (2). This initiates the water-exit phase of the VLFS. Once the water front has passed the pressure probe, the structure becomes dry there and is subjected to atmospheric pressure (3). This lasts until the water starts to rise again and eventually impacts the platform bottom (4). As a result, a water-entry phase occurs and the water run-up in front of the upwave edge is responsible for an increase of pressure. The latter occurs when the impact loads have become negligible. A secondary relative maximum of the pressure occurs when the maximum run-up is reached by the water (5), then a new water run-down occurs again reducing the pressure level. The main pressure trend during the run-up and run-down phases is altered by high-frequency oscillations and jump-like events. These are probably related to excitation of elastic motions by the slamming and to transient phenomena, such us bow-impact events occurring during the water run-down.

4. Conclusions

VLFS bottom-slamming phenomena were studied in the framework of head sea waves and 2-D potential flow theory. An iterative Domain-Decomposition (DD) incorporated a linear-global analysis of the platform with a fully-nonlinear description of slamming events, in order to analyze their mutual influence. The occurrence of air-entrapment during bottom slamming was discussed, the challenges in identifying a proper criterion were highlighted and a possible strategy was indicated. A pressure criterion for slamming phenomena occurring without air entrainment was proposed and successfully validated. The DD method was applied to a 2-D experimental case studied by Yoshimoto et al. (1997) and showed to converge after few iterations. The method was able to capture the global behavior of the measured pressure and explain it in terms of different stages of wave-structure interaction during water-entry and exit phases. The results

obtained support the use of the solver as a tool to help the understanding of bottom-slamming events for VLFS platforms interacting with head sea waves. The numerical investigation suggested a stochastic nature for the pressure peak due to the impact, while a more repeatable behavior was found for the pressure impulse. The latter also showed a promising agreement with the model tests.

Acknowledgments

The present research activity is partially supported by the Centre for Ships and Ocean Structures (CeSOS), NTNU, Trondheim, within the ''Violent Water-Vessel Interactions and Related Structural Loads'' project, and partially done within the framework of the ''Programma di Ricerca sulla Sicurezza'' funded by *Ministero Infrastrutture e Trasporti*.

References

Faltinsen, O.M., Landrini, M., Greco, M., 2004. Slamming in marine application. Journal of Engineering Mathematics 48, 187–217.

Greco, M., Colicchio, G., Faltinsen, O.M., 2006. Local and global hydroelastic analysis of a VLFS. In: Fourth International Conference on Hydroelasticity in Marine Technology, Wuxi, China, pp. 225–234.

Greco, M., Colicchio, G., Faltinsen, O.M., 2008. Bottom slamming for a very large floating structure: uncoupled global and slamming analyses. Journal of Fluids and Structures, this issue, doi:10.1016/j.jfluidstructs.2008.09.002.

Wagner, H., 1932. Über stoss- und gleitvorgange an der oberflache von flussigkeiten. ZAMM 12 (4), 192–235.

Yoshimoto, H., Ohmatsu, K., Ohmatsuandi, S., Ikebuchi, T., 1997. Slamming load on a very large floating structure with shallow draft. Journal of Marine Science and Technology 2, 163–172.